Binary Classification of Superparamagnetic Relaxometry Data for Cancer Screening

Javad Sovizi, David Fuentes, Sara L. Thrower, Wolfgang Stefan, John D. Hazle, Kelsey B. Mathieu

Department of Imaging Physics, The University of Texas M. D. Anderson Cancer Center, Houston, TX

THE UNIVERSITY OF TEXAS MD Anderson Cancer Center

Making Cancer History®

Introduction

- Superparamagnetic relaxometry (SPMR) is an emerging technology that holds potential for use as a second-line screening modality to improve early cancer detection.
- Measurement of the magnetic field after the excitation of cancer-bound superparamagnetic iron oxide nanoparticles (SPIONs) enables the reconstruction of SPIONs spatial distribution and hence tumor detection.
- **Challenges:**
  - Image reconstruction requires solving an ill-posed inverse problem.
  - Additional image processing module is required to automatically detect and localize the tumor.
- **Approach:**
  Direct classification of the SPMR signal (without image reconstruction) using data-driven Gaussian process (GP) method.

SPMR Measurement

The device used in our study was a 7-channel pre-clinical magnetic relaxometry system (MagSense, Imagion Biosystems, Inc.), shown in Fig. 1 (a).

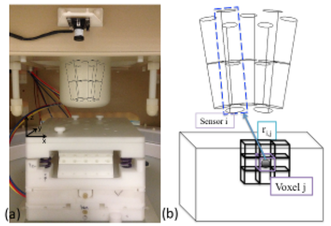

Figure 1: (a) MagSense device (Imagion Biosystems, Inc.). (b) Schematic of forward model described in Eq. (1)

- *Excitation phase*: SPIONs are excited using an external field generated by a Helmholtz magnetizing coil.
- *Relaxation phase*: Sensitive superconducting quantum interference devices (SQUIDs) are switched on to detect the decay of magnetic moment induced by excited SPIONs.

$$\boldsymbol{b} = A\boldsymbol{x} + \boldsymbol{\nu} \qquad (1)$$

$\boldsymbol{b}$: Vector of relaxation amplitudes, *i.e.,* the difference in the magnetic field before and after relaxation.

$\boldsymbol{x}$: Vector of magnetic moments at voxels shown in Fig. 1 (b).

A : System transformation matrix

ν : measurement noise

Gaussian Process Classification

A GP model is trained with several samples of *in silico* or phantom measurements labeled with their class (+1 for with and -1 for without surrogate tumor source). The probability of classes can then be obtained for a new SPMR measurement.

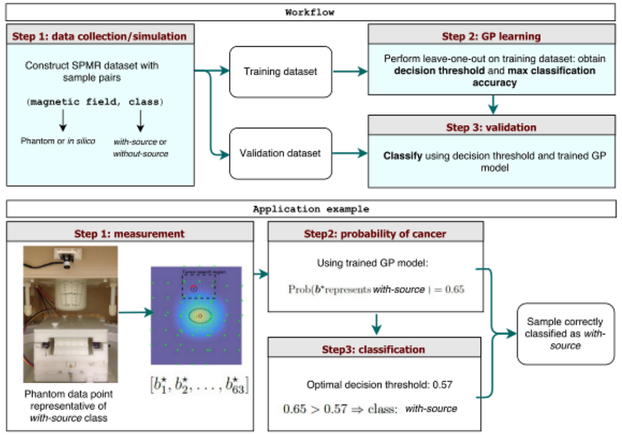

Figure 2: Top panel: the workflow of training and validation of a GP classification model. Bottom panel: An example GP classifier application.

Compressed Sensing Approach

Image reconstruction (ImR) can be performed based on compressed sensing method and the surrogate tumor source can be detected and localized by processing the reconstructed image.

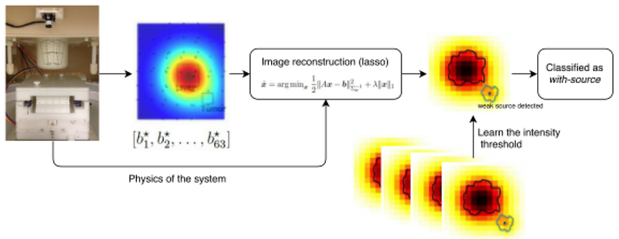

Figure 3: ImR based classification approach. A lasso estimate of moment vector is obtained and the resulting image is processed to detect the surrogate tumor source.

Results

***In silico* studies:**

- Forward model (Eq. (1)) was used to generate SPMR signals
- The geometry and source locations are consistent with the pre-clinical mouse cancer model.
- Several samples of SPMR measurements were generated for evaluating both classification approaches.

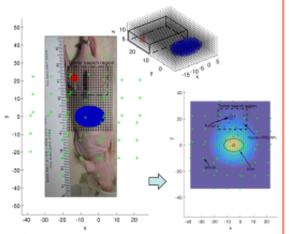

Figure 4: *In silico* signal generation setup.

Classification accuracy:

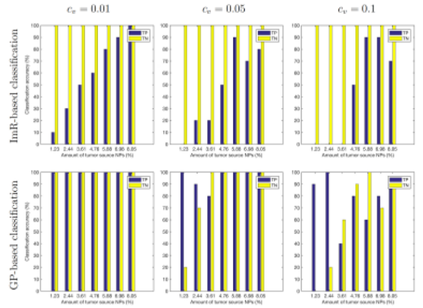

Figure 5: True positive (TP) and false negative (FN) rates when there is **no background SPIONs**. c_v is the coefficient of variation (relative standard deviation) of the measurement noise.

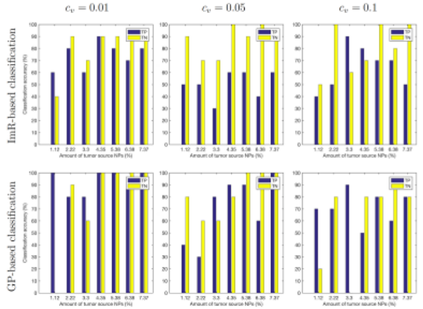

Figure 6: True positive (TP) and false negative (FN) rates when **8-9% background SPIONs** are randomly distributed.

Phantom studies:

- The strong source (surrogate liver) was simulated by clustering together nine cotton swabs containing a total of 150 μg of immobilized 25-nm Fe_3O_4 SPIONs (PrecisionMRX; Imagion Biosystems).
- The weak source (surrogate tumor) was represented by a single cotton swab containing either 6.3, 9.4, or 14.4 μg of immobilized PrecisionMRX SPIONs.
- An additional nine cotton swabs containing a total of 32 μg of immobilized PrecisionMRX SPIONs (<5 μg per swab) were evenly distributed within the scan plane to represent background SPIONs.

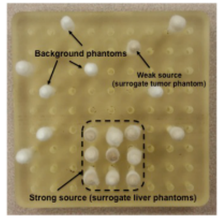

Figure 7: Phantom experiment setup

- We collected 14 data points by moving tumor phantom to 14 different positions. Also, 10 additional data points were collected without using the tumor phantom.

Classification accuracy: GP vs ImR approach

Weak source phantom: 14.44 μg

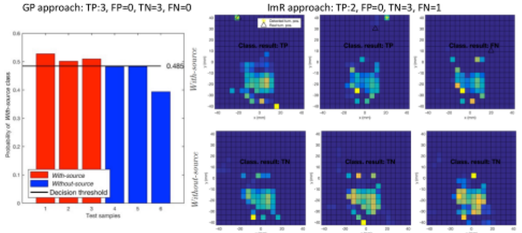

Figure 8: GP-based (left panel) and ImR-based (right panel) classification results when 14.44 μg surrogate tumor phantom is used.

Weak source phantom: 9.4 μg

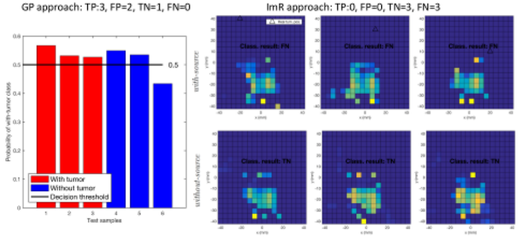

Figure 9: GP-based (left panel) and ImR-based (right panel) classification results when 9.4 μg surrogate tumor phantom is used.

Conclusion

- In our *in silico* source detection analysis, and for realistic noise levels, we were able to achieve overall classification accuracies above 90% when >5% of total SPIONs were concentrated at the surrogate tumor.
- In our phantom studies, we were able to detect the surrogate tumor phantoms with 5% and 7.3% of the total used SPIONs, surrounded by 9 low-concentration phantoms with accuracies of 87.5% and 96.4%, respectively.
- The GP framework provides acceptable classification accuracies when dealing with *in silico* and phantom SPMR datasets and can outperform an image reconstruction method for binary classification of SPMR data.
- In addition to measurement noise, existence of the background SPIONs can reduce the classification accuracies in both ImR and GP based approaches.
- **Future work:**
  - Prior knowledge of the SPIONs distribution can significantly improve the classification accuracy. This necessitates development of a biodistribution kinetics model and integration of the model into classification framework for *in vivo* applications.
  - Since the concentration of tumor-bound SPIONs may be very low for small tumors at the early stage of the cancer, more advanced deep learning techniques should be implemented to reliably classify SPMR measurements.

References

1) Rasmussen, C.E., 2006. Gaussian processes for machine learning.

2) R.G. Baraniuk, Compressive sensing [lecture notes], IEEE signal processing magazine , 2007.

3) Flynn, E.R. and Bryant, H.C., 2005. A biomagnetic system for in vivo cancer imaging. Physics in medicine and biology, 50(6), p.1273.

4) Blanco, E., Shen, H. and Ferrari, M., 2015. Principles of nanoparticle design for overcoming biological barriers to drug delivery. Nature biotechnology, 33(9), pp.941-951.

5) Peracchia, M.T., Fattal, E., Desmaele, D., Besnard, M., Noel, J.P., Gomis, J.M., Appel, M., d'Angelo, J. and Couvreur, P., 1999. Stealth® PEGylated polycyanoacrylate nanoparticles for intravenous administration and splenic targeting. Journal of Controlled Release, 60(1), pp.121-128.

6) Wiekhorst, F., Seliger, C., Jurgons, R., Steinhoff, U., Eberbeck, D., Trahms, L. and Alexiou, C., 2006. Quantification of magnetic nanoparticles by magnetorelaxometry and comparison to histology after magnetic drug targeting. Journal of nanoscience and nanotechnology, 6(9-1), pp.3222-3225.

7) Richter, H., Kettering, M., Wiekhorst, F., Steinhoff, U., Hilger, I. and Trahms, L., 2010. Magnetorelaxometry for localization and quantification of magnetic nanoparticles for thermal ablation studies. Physics in medicine and biology, 55(3), p.623.

8) Loupot, S., Stefan, W., Madankan, R., Mathieu, K. B., Fuentes, D., Hazle, J. D., 2016. Sparse Source Reconstruction for Nanomagnetic Relaxometry, International Workshop on Magnetic Particle Imaging (IWMPI).